NLRP3 inflammasome-mediated cerebrospinal fluid hypersecretion in choroid plexus contributes to hydrocephalus after hemorrhage

Zhaoqi Zhang
Department of Neurosurgery, Southwest Hospital, Army Medical University
Qiang Tan
Department of Neurosurgery, Southwest Hospital, Army Medical University
Peiwen Guo
Department of Neurosurgery,Southwest Hospital, Army Medical University
Zhengcai Jia
Department of Neurosurgery, Southwest Hospital, Army Medical University
Xin Liu
Department of Neurosurgery, Southwest Hospital, Army Medical University
Hua Feng (fenghua8888@vip.163.com)
Southwest Hospital, Third Military Medical University (Army Medical University) https://orcid.org/0000-0003-4489-9217

Research

Keywords: NLRP3 inflammasome, Choroid plexus, NKCC1, CSF secretion, Hydrocephalus

Posted Date: November 20th, 2020

DOI: https://doi.org/10.21203/rs.3.rs-109549/v1

Abstract

Background

Hydrocephalus is a severe complication of intracerebral hemorrhage with ventricular extension (ICH-IVH). The choroid plexus epithelium plays an important role in cerebrospinal fluid (CSF) secretion and constitutes blood-CSF barrier adjusting brain–immune system interface. NLRP3 inflammasome is a key component of the innate system which promotes neuroinflammation. However, the role of NLRP3 inflammasome in the pathogenesis of hydrocephalus after hemorrhage has not been investigated.

Methods

Hydrocephalus after ICH-IVH rat model was accomplished by autologous blood infusion. Then, we investigated the relationship between NLRP3 inflammasome and CSF hypersecretion in choroid plexus.

Results

The NLRP3 inflammasome activated and CSF hypersecretion in choroid plexus epithelium were found after ICH-IVH. NLRP3 inhibition with MCC950 decreased CSF secretion, ventricles dilation and attenuated neurofunction deficits after ICH-IVH. In addition, MCC950 decreased NKCC1 phosphorylation which was the major protein adjusting CSF secretion and improved blood-CSF barrier integrity after ICH-IVH.

Conclusions

This study demonstrates that NLRP3 inflammasome mediated CSF hypersecretion by influencing NKCC1 phosphorylation in choroid plexus epithelium plays an important role in the pathogenesis of hydrocephalus after hemorrhage and provides a new therapeutic strategy.

Background

Intracerebral hemorrhage (ICH) occurs in 10-15% of all strokes worldwide each year[1]. About 40% intracerebral hemorrhage patients combine intraventricular hemorrhage, among which 50% will develop into hydrocephalus[2, 3]. Extension to ventricles after ICH is an independent factor to hydrocephalus[4]. Persistent elevations in intracranial pressure can cause acute brainstem herniation and death[5]. Invasive CSF shunting remains the treatment for hydrocephalus after hemorrhage, but which occurred many complications such as shunt obstructions or infections[6, 7]. It is necessary to find targeted pharmacotherapeutic strategies to patients with hydrocephalus[8].

CSF circulation failed is the major mechanism for hydrocephalus after hemorrhage widely accepted. Most of the studies aim to CSF flowing out obstacles. After hemorrhage, the ependymal glia and arachnoid granulations dysfunction aggravated hydrocephalus[9, 10]. TLR4–dependent inflammatory response contributes to hydrocephalus through CSF hypersecretion[11]. The CSF is predominantly produced by the choroid plexus, an epithelial monolayer which is the main component of the blood-CSF

barrier[12, 13]. The $Na^+/K^+/2Cl^-$cotransporter (NKCC1) expressed in the luminal membrane of choroid plexus contributes approximately half of the CSF production[14]. As one chloride importer antagonist of NKCC1, bumetanide attenuates many neurological and psychiatric disorders. Blood metabolites intracerebroventricular injection caused choroid plexus inflammation and hydrocephalus but the mechanisms remain unclear. Secretory epithelia can respond to proinflammatory stimulation by increasing fluid secretion rate.

The NLRP3 inflammasome as a critical component of the innate immune response to tissue injury, which could release cytokines and exacerbated brain edema after ICH. MCC950 is the specific inhibitor of NLRP3 inflammasome which reduces brain injury after hemorrhage.

However, the pathogenesis of hydrocephalus after hemorrhage still are limited to explain. Therefore, we hypothesized that NLRP3 could aggravate hydrocephalus after ICH-IVH via enhancing CSF secretion in choroid plexus. The present study set out to test the function and molecular mechanism of NLRP3 inflammasome in the pathogenesis of hydrocephalus, then find a new therapeutic target for hydrocephalus patients.

Methods

Animals

Adult male Sprague-Dawley rats (220g-250g;) were purchased from the Army Medical university and kept on a feedback-controlled heating pad to maintain body temperature at 37.0℃. Animal using procedures was in compliance with the guide for the care and use of laboratory animals and approved by the animal care and use committee at the Army Medical university (SCXK-PLA-20120011).

ICH-IVH Model of hydrocephalus and drug treatment

The surgical procedures for rats subjected to hemorrhage were well described in our previous study[9, 15]. In brief, animals were anesthetized with pentobarbital (40 mg/kg intraperitoneal). The right femoral artery was catheterized as a source of blood sample. The rats were positioned in a stereotaxic frame, a cranial burr hole (1 mm) was drilled (coordinates:0.2 mm posterior and 2.2 mm lateral to the bregma). A 29-gauge needle was inserted at a rate of 1mm/min at the depth of 5.0 mm from the dura. Using a microinjection pump, 200μl nonheparinized arterial blood was infused into the right caudate nucleus at a rate of 14μl/min through the hole. Normal saline was infused as vehicle groups. NLRP3 inhibitor MCC950 (MCE, USA) dissolved in normal saline was administered by intraperitoneal injection 1 hour after ICH-IVH at a dose of 10mg/kg. Bumetanide (MCE, USA) dissolved in normal saline was administered by intraperitoneal injection each day after ICH-IVH at a dose of 10mg/kg.

Brain water content

Three days after blood infusion, rats were euthanized without perfusion. Brains were removed immediately and divided into three parts: left-hemisphere, right-hemisphere and cerebellum. Firstly, the wet weights were measured using fresh tissue. Then, the brain sections were dried at 100℃ for 24 hours before obtaining the dry weights. The percentage brain water content was calculated as follows formula: (wet weight–dry weight)/wet weight100.

Neurobehavioral examination

Neurological dysfunction of rats was evaluated using a modified Neurological Severity Score (mNSS) method as described previously[16]. Briefly, the assessment was performed at 3 and 7 days after ICH-IVH. First, the mNSS are a composite test of motor, sensory, and balance functions. Neurological function was graded on a scale of 0-18 (a score of 13-18 indicates severe injury, 7-12 indicates moderate injury, and 1-6 indicates mild injury).

Qualification of CSF secretion rate

Rates of CSF production were measured using the method as previously described[17]. Briefly, anesthetized rats were mounted on a stereotactic apparatus, and a cranial burr hole (1.2 mm) was drilled over the left lateral ventricle (coordinates, relative to the bregma: x, -0.6cm; y, -1.6cm). Next, the rat's head was rotated on the ear-bars by 90° so that it was oriented nose down, and the suboccipital muscles were dissected to the cisterna magna to expose the atlantooccipital ligament. The ligament was punctured, and a 29-gauge needle was advanced 5 mm through the foramen of Magendie to the fourth ventricle. Sterile molecular-grade oil (100μl; Sigma-Aldrich) was infused through the tube to occlude the aqueduct of sylvius, thereby creating a closed system of CSF circulation in lateral ventricle. With the rat in the same position, a glass capillary tube (OD,1.1mm; ID,1.0mm; length,20cm) was advanced through the burr hole into the lateral ventricle (depth 4.5mm ventral). The volume of CSF that collected at a given time (20 min) was calculated as: V (mm3) $=\pi \cdot r^2 \cdot d$, where r is the radius of the glass capillary tube and d is the distance that CSF traveled within the capillary. The rate of CSF formation (μl/min) could be calculated from the slope of volume-time relationship.

Transmission electron microscope

Electron microscopy was performed as previously described[18]. Rats were anesthetized and subjected to intracardiac perfusion with 4% paraformaldehyde and 2.5% glutaraldehyde in 0.1mol/L Sorensen's buffer (pH 7.4). The choroid plexus were removed from brain and a 1-mm-thick coronal tissue slice was cut with a blade 4 mm overnight at 4°C. Samples were then post-fixed with 1.0% OsO4 and dehydrated in graded ethyl alcohol. After completion of dehydration, samples were infiltrated with propylene oxide, embedded in Epon resin, and sectioned. Ultra-thin sections were then stained with uranyl acetate and Reynold's lead citrate. Sections were evaluated using a Philips CM 100 transmission electron microscope (Hillsboro, OR, USA) and digitally acquired using a Hamamatsu (Hamamatsu City, Shizuoka, Japan) ORCA-HR camera.

Blood-CSF Barrier permeability measurement

CSF was obtained at 3 days after blood infusion by puncture of the cisterna magna and stored at -80℃ prior to analysis, and dextran-10,000 MW (Invitrogen, USA) was given by vein 2 hours before collecting CSF. CSF was measured absorbance at 540nm using Spectrophotometer.

Western blot analysis

Western blot analysis was performed as previously described[19]. The brains were perfused with saline before decapitation at day 3 after injection. The choroid plexus tissue was sampled. The following primary antibodies were used: rabbit anti-NLRP3 (1:1000 dilution, Abcam, UK), mouse anti-Caspase-1 (1:1000 dilution, Novus, USA), rabbit anti-IL-1beta (1:1000 dilution, Gene-Tex, USA), rabbit anti-p-NKCC1 (1:1000 dilution, Sigma-Aldrich, USA) , rabbit anti-NKCC1 (1:1000 dilution, CST, USA), rabbit anti-ZO-1 (1:5000 dilution, Abcam, UK) ,and rabbit anti-β-actin(1:1000 dilution, CST, USA). The relative densities of the immune-reactive bands were normalized to β-actin and analyzed using ImageJ (National Institutes of Health, Bethesda, Maryland, USA).

Cytokines Assay Kits

Rats were anaesthetized with pentobarbital (40 mg/kg intraperitoneal). CSF was collected through the cisterna magna, then rats were decapitated to get the choroid plexus. The CSF was centrifuged at 10,000 rpm to separate the supernatant. The choroid plexus were homogenized in ice-cold PBS with protease inhibitor cocktails (Sigma-Aldrich, USA). Total protein concentration was quantified by the BCA protein assay (Boster, China). The CSF and choroid plexus cytokines levels were measured using inflammation cytokines assay kits (Raybiotech, USA) according to the manufacturer's instructions.

Immunofluorescence staining

Immunofluorescence staining of brain tissue was performed on fixed frozen sections as previously described. Rats were anesthetized with pentobarbital (40 mg/kg intraperitoneal) and perfused with 4% paraformaldehyde for 4 to 6 hours. The brain was isolated and then dissected the choroid plexus under magnification using sharp forceps. The choroid plexus were immersed in 30% sucrose for 3 to 4 days at 4℃. The tissues were embedded in an optimal cutting temperature compound (SAKURA, USA), and 12-mm-thick slices were cut using a cryostat. The slices were incubated with the following primary antibodies at 4℃ overnight: rabbit antibody to NLRP3(1:200, Abcam, UK), rabbit antibody to p-NKCC1(1:200 dilution, Sigma-Aldrich, USA). Then the slices were probed with appropriate secondary antibodies for 2 h at 37 °C. Finally, the slices were counterstained with DAPI (Boster, China) and examined using a confocal fluorescence micro- scope (LSM780, Zeiss).

Cell counts

The cell counts were performed at day 3 after ICH-IVH, respectively. Cell counts analysis was performed as previously described. For quantification of the positive cells in the choroid plexus, consecutive slices were made, and two sections per animal (n=6 per group) with 40-μm space in between were used for cell counts. Three high-power images were used for cell counting. NLRP3 and p-NKCC1 positive cells were

counted in the choroid plexus. Cell counts were performed by two researchers in a blinded manner. All measurements were repeated three times, and the mean value were used.

MRI and ventricular volume analysis

Rats were anesthetized with 2% isoflurane/air mixture throughout MRI examination. The MRI scans were performed in a 7.0-T Varian MR scanner (Bruker, USA) with a T2*gradient-echo sequence and a T2 fasts spin-echo sequence using a view field of 35mm*35mm and 17 coronal slices (1.0mm thickness). Volumes were calculated as previously described[20]. Bilateral ventricles and hippocampus were outlined, and the areas of all slices and multiplying by the section thickness[21]. All image analyses were performed using Image J (National Institutes of Health, Bethesda, Maryland, USA) by two observers in blinded manner.

Statistical analysis

The values in this study are presented as mean ± SD. SPSS 19.0 software was used to analysis all data. Data were analyzed by Student t test for single comparisons or ANOVA with post hoc Bonferroni-Dunn correction for multiple comparisons. A P value of <0.05 was considered statistically significant.

Results

ICH-IVH aroused CSF hypersecretion，hydrocephalus and neurocognitive functional deficits

3 days after blood infusion, the frozen sections and T2 MRIs showed ICH-VIH group more severer lateral ventricle dilation than vehicle group (Fig.1A), and using the T2 MRIs images to quantitative measure the lateral ventricle volume got the same conclusion (9.58±1.16 versus 38.17±4.3 mm^3; P<0.01; Fig.1C).The brain water content of the ipsilateral hemisphere in the ICH-IVH group was much higher than which in vehicle group(77.97±0.65 versus 78.58±1.32; P<0.01; Fig.1B). The CSF secretion rate of ICH-IVH group was much higher than that in the vehicle group at 3 and 7 days (3 days: 0.93±0.21 versus 2.62±0.53 μl/min; 7 days: 0.42±0.17 versus 0.93±0.14 μl/min; P<0.01; Fig.1D). In addition, the mNSS used to evaluate the neurofunction showed ICH-IVH group had more obvious loss of neurofunction than vehicle group at 3 and 7 days (Fig.1E). We observed hydrocephalus and CSF hypersecretion after ICH-IVH.

NLRP3 inflammasome components were activated in choroid plexus and CSF after ICH-IVH

At 3 days after ICH-IVH, we found more NLRP3 positive cells in choroid plexus than vehicle group (Fig.2A and Fig.2C). In addition, the protein expression of NLRP3, Caspase-1, and IL-1beta of ICH-IVH group were much higher than vehicle group in choroid plexus (Fig.2B and Fig.2D-2F). Using cytokine assay kits we found that reported NLRP3 related cytokine factors IL-1beta and IL-18 were much higher after ICH-IVH in choroid plexus (Fig.6D and Fig.6E). Compared with vehicle group, IL-1beta and IL-18 also had higher protein expression in CSF (Fig.6A and Fig.6B). According to assay kits results, many inflammation related cytokines increased after ICH-IVH both in choroid plexus and CSF (Fig.S1). These results demonstrated that NLRP3 inflammasome components were activated after ICH-IVH.

MCC950 reduced NLRP3 inflammasome components levels, ameliorated hydrocephalus and improved neurofunction

MCC950 is a NLRP3 specific inhibitor, which could lessen the lateral ventricle volume after ICH-IVH (38.17±4.3 versus 29±3.41 mm^3; P<0.01; Fig.3A and Fig.3B). The brain water contents in ICH-IVH group also severe reduced than MCC950 group (78.58±1.32 versus 78.95±0.95; P<0.05; Fig.3C). Compared with ICH-IVH group, we found that MCC950 treated rats had significantly reduced neurofunction deficits (Fig.3G) and CSF secretion rates at 3 and 7 days (3 days: 2.62±0.53 versus 2.05±0.23 μl/min; 7 days: 0.93±0.14 versus 0.73±0.14 μl/min; P<0.02; Fig.3F). In the choroid plexus, we found MCC950 treated reduced the NLRP3 positive cells after ICH-IVH (Fig.3D and Fig.3E). Then, the protein expression of NLRP3, Caspase-1, and IL-1beta after MCC950 treated were much lower than ICH-IVH group in choroid plexus (Fig.2H and Fig.2I-2K). According to cytokines assay kits results, IL-1beta and IL-18 protein expression reduced after MCC950 treated both in choroid plexus and CSF (Fig.6A-B and Fig. 6D-E). In addition, MCP-1, IL-6, and TNF-alpha also decreased after MCC950 treated (Fig.S1).

MCC950 decreased NKCC1 phosphorylation after ICH-IVH

3 days after ICH-IVH, more p-NKCC1 positive cells were found in ICH-IVH group than vehicle group, and MCC950 treated decreased p-NKCC1 positive cells in choroid plexus (Fig.4A and Fig.4C). Compared with vehicle group, the protein expression of p-NKCC1 was reduced by MCC950 after ICH-IVH (Fig.4B and Fig.4D). Based on these, we presume NKCC1 is related to NLRP3 inflammasome.

Bumetanide reduced NKCC1 phosphorylation and decreased CSF secretion rate but no function to NLRP3

Bumetanide is a NKCC1 specific inhibitor, which reduced p-NKCC1 positive cells in choroid plexus after ICH-IVH (Fig.5A and Fig.5B). In addition, bumetanide reduced CSF secretion rate after ICH-IVH (3 days: 2.62±0.53 versus 0.96±0.12 μl/min; 7 days: 0.93±0.14 versus 0.44±0.05 μl/min; P<0.01; Fig.5C). The protein expression of p-NKCC1 was reduced by bumetanide after ICH-IVH (Fig.5D and Fig.5E). However, bumetanide treated could not reduce NLRP3 protein expression in choroid plexus after ICH-IVH (Fig.5D and Fig.5F). In a word, bumetanide could decrease CSF secretion rate by inhibiting NKCC1 phosphorylation but not influencing NLRP3.

MCC950 repaired Blood-CSF damages in choroid plexus after ICH-IVH

According to the cytokine assay kits, we found that ICAM-1 higher expressed in ICH-IVH group than vehicle group both in CSF and choroid plexus, and MCC950 treated reduced ICAM-1 protein expression level (Fig.6C and Fig.6F). Then, the dextran-10,000 MW was used to assess the integrity of blood-CSF barrier. ICH-IVH group had more dextran leakage than vehicle group (Fig.7A), and absorbance at 540 nm also supported this result (Fig.7C). TEM images of choroid plexus showed more tight junctions destroyed in ICH-IVH group than vehicle group (Fig.7B). The protein expression of ZO-1 was much lower after ICH-IVH (Fig.7D and Fig.7E). After treated with MCC950, the leakage of dextran and CSF absorbance at 540 nm were ameliorated rather than ICH-IVH group (Fig.7A and Fig.7C). Compared with ICH-IVH group,

MCC950 treated improved tight junctions in TEM images and the protein expression of ZO-1(Fig.7B and Fig.7D-E). This result indicated that tight junctions between choroid plexus epithelial cells and blood-CSF barrier were destroyed which may be a source of CSF after ICH-IVH. These damages contributed to aggravate hydrocephalus and MCC950 treated could repair damaged blood-CSF barriers.

Discussion

In the present study, we show that NLRP3 inflammasome was activated which contributed to hydrocephalus by mediating CSF hypersecretion and damaging blood-CSF barrier in choroid plexus after ICH-IVH. What's more, NLRP3 inflammasome influenced CSF secretion through adjusting NKCC1 phosphorylation in choroid plexus. Together, these results suggest that NLRP3 inflammasome contribute to the pathogenesis of hydrocephalus after ICH-IVH.

The hydrocephalus is a severe complication after ICH especially with ventricles extension[22, 23]. Most studies about hydrocephalus after hemorrhage is based on intraventricular hemorrhage (IVH) model no matter in infants or adults which cannot simulate the clinical pathogenesis of hydrocephalus after hemorrhage[24]. As our previous study, hydrocephalus and brain tissue injury are more serious in a rat model of ICH-IVH than IVH, which is more conformer to the clinical[9]. Therefore, we use ICH-IVH model to explore pathogenesis of hydrocephalus in this study.

It is a commonly held view that hydrocephalus after hemorrhage is due to alterations in the CSF drainage pathway, particularly related to the cerebral aqueduct, fourth ventricular outlets, ependymal epithelium damage, arachnoid villi or granulations, and choroid plexus inflammation. There are few animal studies that actually investigate either the cerebral aqueduct or the outlets of the fourth ventricle. The arachnoid granulations are regarded as sites of absorption. Both the presence and morphology of arachnoid granulations is different between humans and animals[25]. However, the arachnoid granulations still are not completely developed in infants hydrocephalus[26, 27]. After nerve tissue has lymphatic vessels were widely proved[28-30]. It is accepted that a considerable amount of CSF flows into lymphatic vessels and lymphatic outflow may result in hydrocephalus[31]. Beating of the ependymal cilia generates flow of the CSF within the brain cavities and aids in maintaining patency of the ventricular system[32, 33]. The clinical and preclinical data suggest that loss of developing and mature ciliate epithelial cells contribute to hydrocephalus after hemorrhage [34-36]. All of these studies concentrate on the outflow dysfunction of CSF. The choroid plexus located at the base of each of the four ventricles. As for the produce of CSF in choroid plexus, there are few related studies. Nuclear factor κB (NF-κB) signaling was activated by the CSF barrier cells of the choroid plexus and ependymal lining after IVH[37]. Systemic inflammation stimulates TLRs in the choroid plexus, which may lead to disturbances in choroid plexus barrier function[38]. Recently study proved that TLR4-dependent inflammation leads to CSF hypersecretion plays a role in hydrocephalus after hemorrhage[11]. It has been reported that NLRP3 mediated many kinds of nervous system injuries after ICH, subarachnoid hemorrhage, or traumatic brain injury[16, 39], but there are no studies about the NLRP3 inflammasome in hydrocephalus. Based on these, we focus on the NLRP3 inflammasome and choroid plexus, then proved that NLRP3 contributes to hydrocephalus by

increasing CSF secretion in choroid plexus. The method in this study to measure CSF secretion is single, and more ways are needed to explore. Furthermore, Blood components are complex, and which components activated NLRP3 inflammasome in choroid plexus is unclear. Many factors, such as iron, hemoglobin, and transforming growth factor-β1, contribute to hydrocephalus after hemorrhage[9, 40, 41]. Future studies we aim to explore what activates NLRP3 inflammasome after ICH-IVH in choroid plexus.

After we found NLRP3 inflammasome activated after ICH-IVH in choroid plexus, we attempted to find molecular mechanisms between NLRP3 inflammasome and CSF formation. Approximate 500ml fluid is produced by the choroid plexus in the mammalian brain. The CSF production is assumed to take place by transport of osmotically active ions, passive movement of water, and the water channel aquaporin. the $Na^+/K^+/2Cl^-$ cotransporter 1 (NKCC1) and the K^+/Cl^- cotransporters (KCCs) are the main ions transporters adjusting CSF formation, and the NKCC1 plays a decisive role[14, 42, 43]. The CSF production only declined by a mere 20% in the AQP1 knock-out mice[44], AQP4 also contributes to CSF formation, but its function also limited[45]. The main regulation molecule NKCC1 was selected in this study, and it was briefly proved that NKCC1 is one molecular in NLRP3 mediated CSF hypersecretion. Because of limited evidences, further studies are still needed to clarify NLRP3 mediated CSF hypersecretion after ICH-IVH.

The most widely recognized choroid plexus role is as the site of the blood-CSF barrier, controller of the internal CNS microenvironment[46]. Blood-CSF barrier integrity is impaired in the pathology of many common CNS disorders such as Alzheimer's disease, Parkinson's disease and stroke[47]. Neuroinflammation is a part of the response to CNS injury and disease when blood-CSF barrier dysfunction[48]. We found blood-CSF barrier dysfunction after ICH-IVH, and inhibited NLRP3 inflammasome could improve its integrity. The relationship between blood-CSF barrier integrity and NLRP3 inflammasome is needed to explore.

In this study, we observed that ICH-IVH induced CSF hypersecretion and blood-CSF barrier disruption by activating NLRP3 inflammasome, and the ion cotransporter NKCC1 regulating CSF secretion also participated in this process. In addition, we found lipid droplets formation in the choroid plexus by accident. Lipid droplets (LDs) are the major lipid storage organelles of eukaryotic cells which are central players in anti-infection[49]. Our further studies will focus on what components in blood contribute to NLRP3 inflammasome activation and LDs formation. Although we found a new therapeutic target for hydrocephalus after hemorrhage, but the pathogenesis of hydrocephalus still needed to explore.

Conclusion

Our results showed that NLRP3 activated in choroid plexus contributed to CSF higher-secretion and aggravated hydrocephalus after ICH-IVH, and NLRP3 impacted CSF secretion by regulating NKCC1 phosphorylation level. In addition, blood-CSF barrier permeability damaged by NLRP3 activated in choroid plexus after ICH-IVH, which also contributed to aggravate hydrocephalus. This study provides evidence that inhibiting NLRP3 may be a potential therapeutic for preventing hydrocephalus after ICH-IVH.

Declarations

Funding:

This work was supported by the Grant No. 2014CB541606 (H.F.) from the National Key Basic Research Development Program (973 Program) of China.

Conflicts of interest:

All authors declare that they have no conflicts of interest.

Ethics approval:

All institutional and national guidelines for the care and use of laboratory animals were followed.

Authors' contributions:

HF made substantial contributions to the conception and design. ZQZ performed the experiments and acquired the data. QT and PWG measured the ventricular volume, CSF secretion rate, and brain water content. ZCJ and XL read and revised some parts of the manuscript. All authors read and approved the final manuscript.

References

1. Keep, R.F., Y. Hua, and G. Xi, *Intracerebral haemorrhage: mechanisms of injury and therapeutic targets.* Lancet Neurol, 2012. **11**(8): p. 720-31.
2. Mustanoja, S., et al., *Extent of secondary intraventricular hemorrhage is an independent predictor of outcomes in intracerebral hemorrhage: data from the Helsinki ICH Study.* Int J Stroke, 2015. **10**(4): p. 576-81.
3. Hallevi, H., et al., *Intraventricular hemorrhage: Anatomic relationships and clinical implications.* Neurology, 2008. **70**(11): p. 848-52.
4. Hu, R., et al., *Long-term Outcomes and Risk Factors Related to Hydrocephalus After Intracerebral Hemorrhage.* Transl Stroke Res, 2020.
5. Dmello, D., S. Cruz-Flores, and G.M. Matuschak, *Moderate hypothermia with intracranial pressure monitoring as a therapeutic paradigm for the management of acute liver failure: a systematic review.* Intensive Care Med, 2010. **36**(2): p. 210-3.
6. Kahle, K.T., et al., *Hydrocephalus in children.* Lancet, 2016. **387**(10020): p. 788-99.
7. Santucci, J.A., et al., *Radiological Estimation of Intracranial Blood Volume and Occurrence of Hydrocephalus Determines Stress-Induced Hyperglycemia After Aneurysmal Subarachnoid Hemorrhage.* Transl Stroke Res, 2018.
8. McAllister, J.P., 2nd, et al., *An update on research priorities in hydrocephalus: overview of the third National Institutes of Health-sponsored symposium "Opportunities for Hydrocephalus Research:*

Pathways to Better Outcomes". J Neurosurg, 2015. **123**(6): p. 1427-38.

9. Chen, Q., et al., *Intracerebral Hematoma Contributes to Hydrocephalus After Intraventricular Hemorrhage via Aggravating Iron Accumulation.* Stroke, 2015. **46**(10): p. 2902-8.
10. Mondejar, V. and A. Patsalides, *The Role of Arachnoid Granulations and the Glymphatic System in the Pathophysiology of Idiopathic Intracranial Hypertension.* Curr Neurol Neurosci Rep, 2020. **20**(7): p. 20.
11. Karimy, J.K., et al., *Inflammation-dependent cerebrospinal fluid hypersecretion by the choroid plexus epithelium in posthemorrhagic hydrocephalus.* Nat Med, 2017. **23**(8): p. 997-1003.
12. Hallaert, G.G., et al., *Endoscopic coagulation of choroid plexus hyperplasia.* J Neurosurg Pediatr, 2012. **9**(2): p. 169-77.
13. Spector, R., et al., *A balanced view of choroid plexus structure and function: Focus on adult humans.* Exp Neurol, 2015. **267**: p. 78-86.
14. Steffensen, A.B., et al., *Cotransporter-mediated water transport underlying cerebrospinal fluid formation.* Nat Commun, 2018. **9**(1): p. 2167.
15. Chen, Q., et al., *Chronic hydrocephalus and perihematomal tissue injury developed in a rat model of intracerebral hemorrhage with ventricular extension.* Transl Stroke Res, 2015. **6**(2): p. 125-32.
16. Ren, H., et al., *Selective NLRP3 (Pyrin Domain-Containing Protein 3) Inflammasome Inhibitor Reduces Brain Injury After Intracerebral Hemorrhage.* Stroke, 2018. **49**(1): p. 184-192.
17. Karimy, J.K., et al., *A novel method to study cerebrospinal fluid dynamics in rats.* J Neurosci Methods, 2015. **241**: p. 78-84.
18. Hu, S., et al., *Thrombin-induced autophagy: a potential role in intracerebral hemorrhage.* Brain Res, 2011. **1424**: p. 60-6.
19. Xi, G., et al., *Attenuation of thrombin-induced brain edema by cerebral thrombin preconditioning.* Stroke, 1999. **30**(6): p. 1247-55.
20. Okauchi, M., et al., *Effects of deferoxamine on intracerebral hemorrhage-induced brain injury in aged rats.* Stroke, 2009. **40**(5): p. 1858-63.
21. MacLellan, C.L., et al., *Intracerebral hemorrhage models in rat: comparing collagenase to blood infusion.* J Cereb Blood Flow Metab, 2008. **28**(3): p. 516-25.
22. Balami, J.S. and A.M. Buchan, *Complications of intracerebral haemorrhage.* Lancet Neurol, 2012. **11**(1): p. 101-18.
23. Strahle, J., et al., *Mechanisms of hydrocephalus after neonatal and adult intraventricular hemorrhage.* Transl Stroke Res, 2012. **3**(Suppl 1): p. 25-38.
24. Schlunk, F. and S.M. Greenberg, *The Pathophysiology of Intracerebral Hemorrhage Formation and Expansion.* Transl Stroke Res, 2015. **6**(4): p. 257-63.
25. Mann, J.D., et al., *Regulation of intracranial pressure in rat, dog, and man.* Ann Neurol, 1978. **3**(2): p. 156-65.

26. Mack, J., W. Squier, and J.T. Eastman, *Anatomy and development of the meninges: implications for subdural collections and CSF circulation.* Pediatr Radiol, 2009. **39**(3): p. 200-10.
27. Oi, S. and C. Di Rocco, *Proposal of "evolution theory in cerebrospinal fluid dynamics" and minor pathway hydrocephalus in developing immature brain.* Childs Nerv Syst, 2006. **22**(7): p. 662-9.
28. Johnston, M., et al., *Evidence of connections between cerebrospinal fluid and nasal lymphatic vessels in humans, non-human primates and other mammalian species.* Cerebrospinal Fluid Res, 2004. **1**(1): p. 2.
29. Ludemann, W., et al., *Ultrastructure of the cerebrospinal fluid outflow along the optic nerve into the lymphatic system.* Childs Nerv Syst, 2005. **21**(2): p. 96-103.
30. Zakharov, A., et al., *Integrating the roles of extracranial lymphatics and intracranial veins in cerebrospinal fluid absorption in sheep.* Microvasc Res, 2004. **67**(1): p. 96-104.
31. Nagra, G., et al., *Impaired lymphatic cerebrospinal fluid absorption in a rat model of kaolin-induced communicating hydrocephalus.* Am J Physiol Regul Integr Comp Physiol, 2008. **294**(5): p. R1752-9.
32. Ibanez-Tallon, I., S. Gorokhova, and N. Heintz, *Loss of function of axonemal dynein Mdnah5 causes primary ciliary dyskinesia and hydrocephalus.* Hum Mol Genet, 2002. **11**(6): p. 715-21.
33. Ibanez-Tallon, I., et al., *Dysfunction of axonemal dynein heavy chain Mdnah5 inhibits ependymal flow and reveals a novel mechanism for hydrocephalus formation.* Hum Mol Genet, 2004. **13**(18): p. 2133-41.
34. Wallmeier, J., et al., *Motile ciliopathies.* Nat Rev Dis Primers, 2020. **6**(1): p. 77.
35. Castaneyra-Ruiz, L., et al., *Blood Exposure Causes Ventricular Zone Disruption and Glial Activation In Vitro.* J Neuropathol Exp Neurol, 2018. **77**(9): p. 803-813.
36. McAllister, J.P., et al., *Ventricular Zone Disruption in Human Neonates With Intraventricular Hemorrhage.* J Neuropathol Exp Neurol, 2017. **76**(5): p. 358-375.
37. Simard, P.F., et al., *Inflammation of the choroid plexus and ependymal layer of the ventricle following intraventricular hemorrhage.* Transl Stroke Res, 2011. **2**(2): p. 227-31.
38. Stridh, L., et al., *Regulation of Toll-like receptors in the choroid plexus in the immature brain after systemic inflammatory stimuli.* Transl Stroke Res, 2013. **4**(2): p. 220-7.
39. Kuwar, R., et al., *A novel small molecular NLRP3 inflammasome inhibitor alleviates neuroinflammatory response following traumatic brain injury.* J Neuroinflammation, 2019. **16**(1): p. 81.
40. Gao, C., et al., *Role of red blood cell lysis and iron in hydrocephalus after intraventricular hemorrhage.* J Cereb Blood Flow Metab, 2014. **34**(6): p. 1070-5.
41. Cherian, S., et al., *Transforming growth factor-betas in a rat model of neonatal posthaemorrhagic hydrocephalus.* Neuropathol Appl Neurobiol, 2004. **30**(6): p. 585-600.
42. Hamann, S., et al., *Cotransport of water by the Na+-K+-2Cl(-) cotransporter NKCC1 in mammalian epithelial cells.* J Physiol, 2010. **588**(Pt 21): p. 4089-101.

43. Zeuthen, T., *Cotransport of K+, Cl- and H2O by membrane proteins from choroid plexus epithelium of Necturus maculosus.* J Physiol, 1994. **478 (Pt 2)**: p. 203-19.
44. Oshio, K., et al., *Reduced cerebrospinal fluid production and intracranial pressure in mice lacking choroid plexus water channel Aquaporin-1.* FASEB J, 2005. **19**(1): p. 76-8.
45. Hasan-Olive, M.M., et al., *Loss of perivascular aquaporin-4 in idiopathic normal pressure hydrocephalus.* Glia, 2019. **67**(1): p. 91-100.
46. Liddelow, S.A., *Development of the choroid plexus and blood-CSF barrier.* Front Neurosci, 2015. **9**: p. 32.
47. Neuwelt, E.A., et al., *Engaging neuroscience to advance translational research in brain barrier biology.* Nat Rev Neurosci, 2011. **12**(3): p. 169-82.
48. Daneman, R., et al., *Pericytes are required for blood-brain barrier integrity during embryogenesis.* Nature, 2010. **468**(7323): p. 562-6.
49. Bosch, M., et al., *Mammalian lipid droplets are innate immune hubs integrating cell metabolism and host defense.* Science, 2020. **370**(6514).

Figures

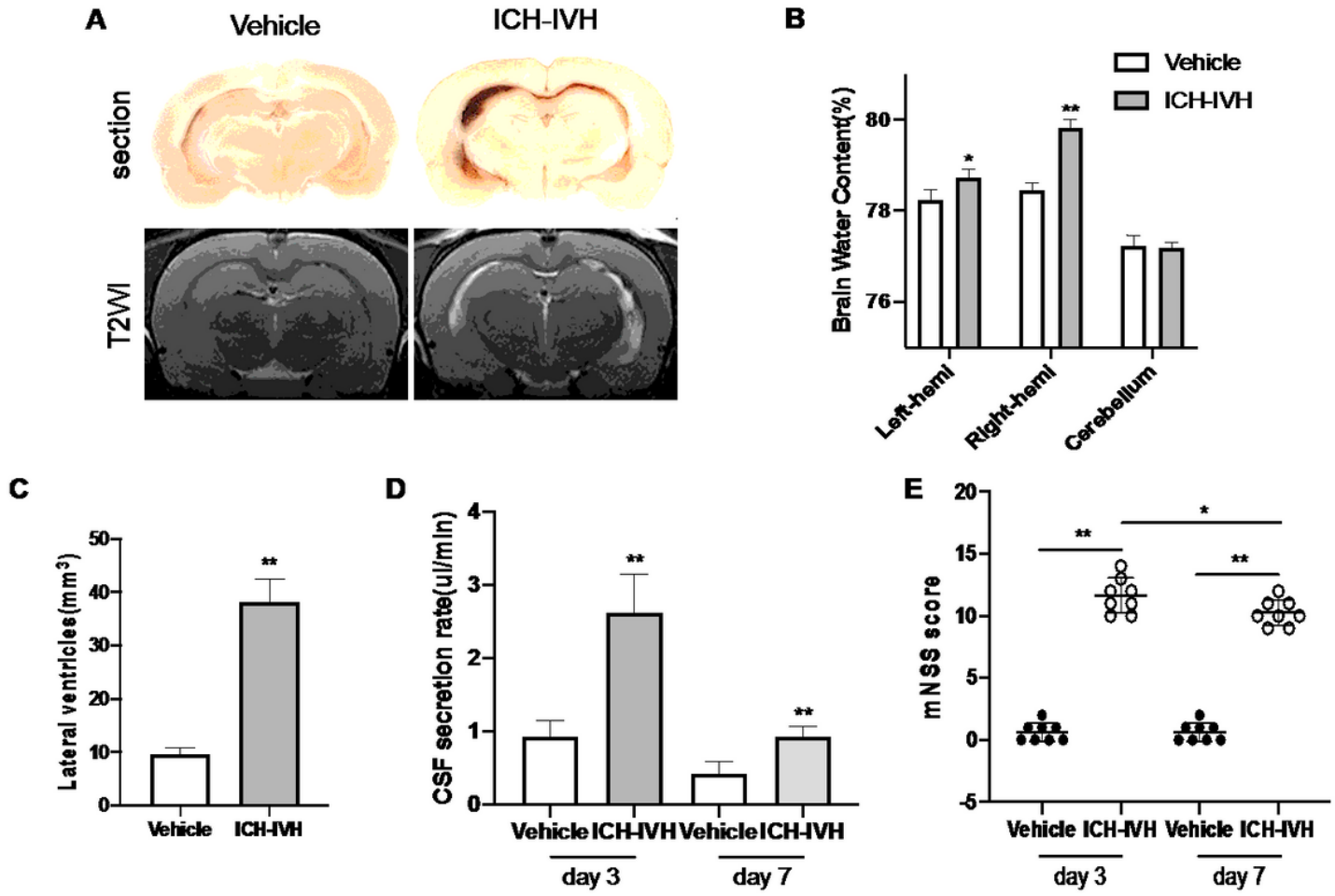

Figure 1

CSF secretion rate and hydrocephalus evaluation index after ICH-IVH. (A) Representative histological section of brain tissue and T2-weighted images obtained at 3 days after ICH-IVH. (C) Quantification volumes of lateral ventricle according to the related T2-weighted images (6 rats/group). (B) Brain water content determination of left, right hemisphere and cerebellum on 3 day after ICH-IVH (6 to 8 rats/group). (D) Quantification CSF secretion rates in vehicle rats and in 3 days, 7 days after ICH-IVH (6-8 rats/group). (E) mNSS (8 rats/group). Results are presented as mean ± SD, **P < 0.01, *P < 0.05.

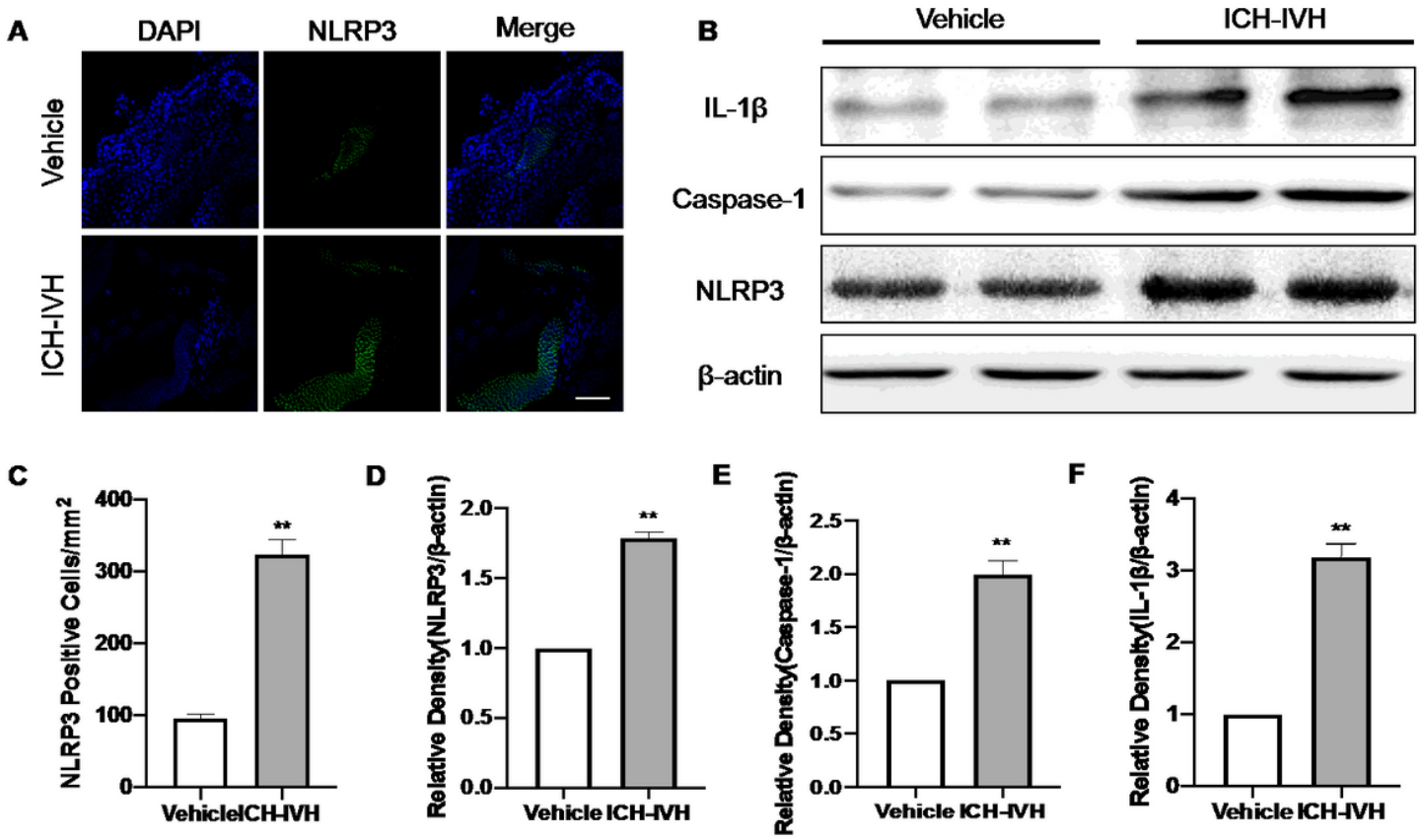

Figure 2

NLRP3 inflammasome components were activated after ICH-IVH in choroid plexus. (A, B) Representative fluorescence photomicrographs showing immunolabeling for NLRP3 (A) and statistical analysis (B) of the cell counting of the NLRP3-positive cells on 3 days after ICH-IVH (6 rats/group). Bar=50μm. (C to F) Western blot analysis of NLRP3, Caspase-1, and IL-1beta in choroid plexus of vehicle rats and ICH-IVH rats at 3 days (8 rats/group). Values are expressed as mean ± SD, **P < 0.01.

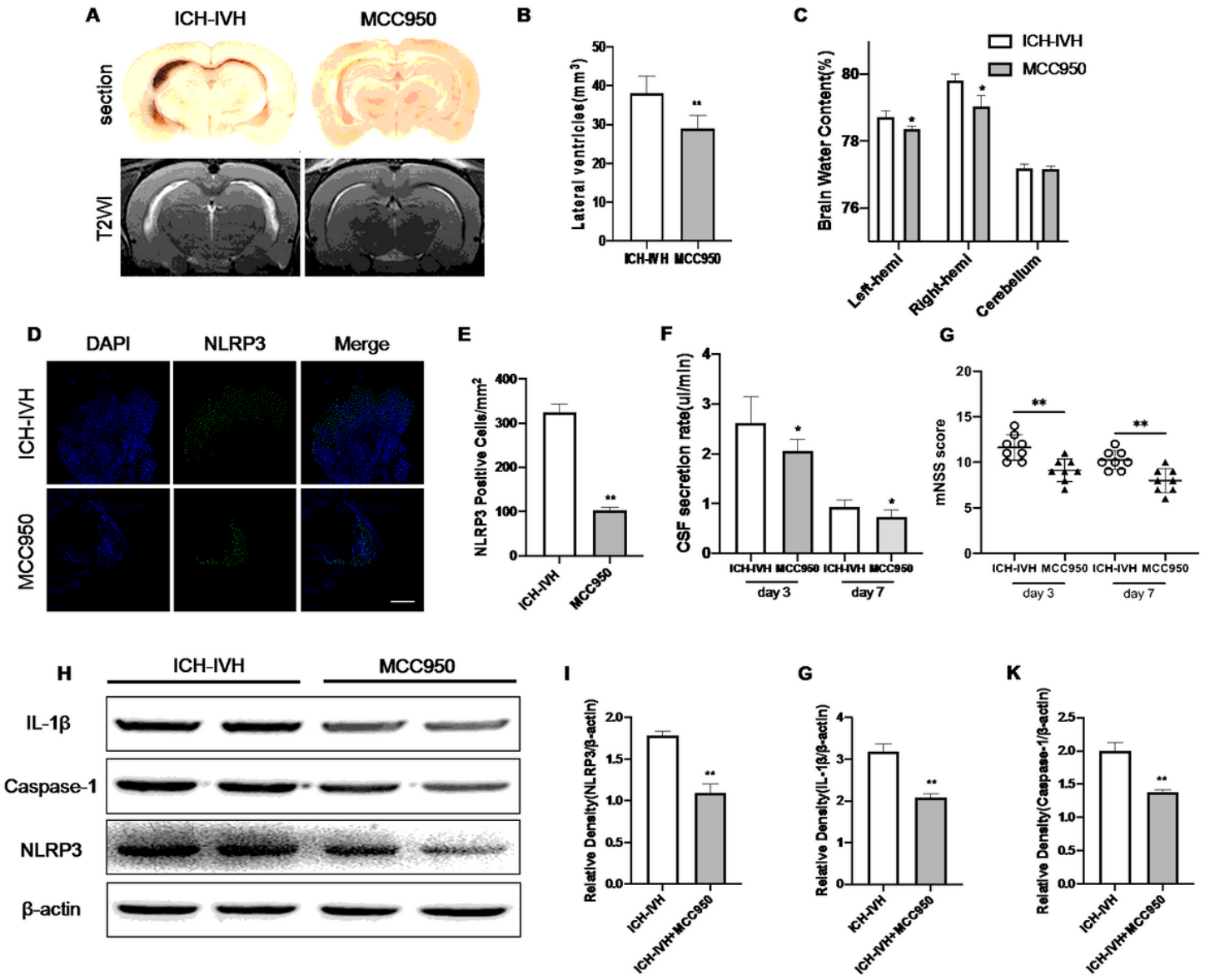

Figure 3

MCC950 decreased NLRP3 related inflammation and hydrocephalus. (A, B) Representative histological section of brain tissue and T2-weighted images after MCC950 treated (A) and lateral ventricle volumes (B) measured by T2-weighted images (6 rats/group). (C) Brain water content on 3 days after MCC950 treated (6 to 8 rats/group). (D, E) Representative photographs of immunofluorescence staining for NLRP3 expression treated (D) and statistical analysis. Bar=50μm. (E) of the cell counting of the NLRP3-positive cells in the choroid plexus 3 days following MCC950 (6 rats/group). (F) Quantification CSF secretion rates in vehicle rats and in 3 days, 7 days after MCC950 treated (6-8 rats/group). (G) mNSS (8 rats/group). (H to K) Western blot analysis of NLRP3, Caspase-1, and IL-1beta in choroid plexus of ICH-IVH rats and MCC950 treated rats at 3 days (6 rats/group). Values are expressed as mean ± SD, **P < 0.01, *P < 0.01.

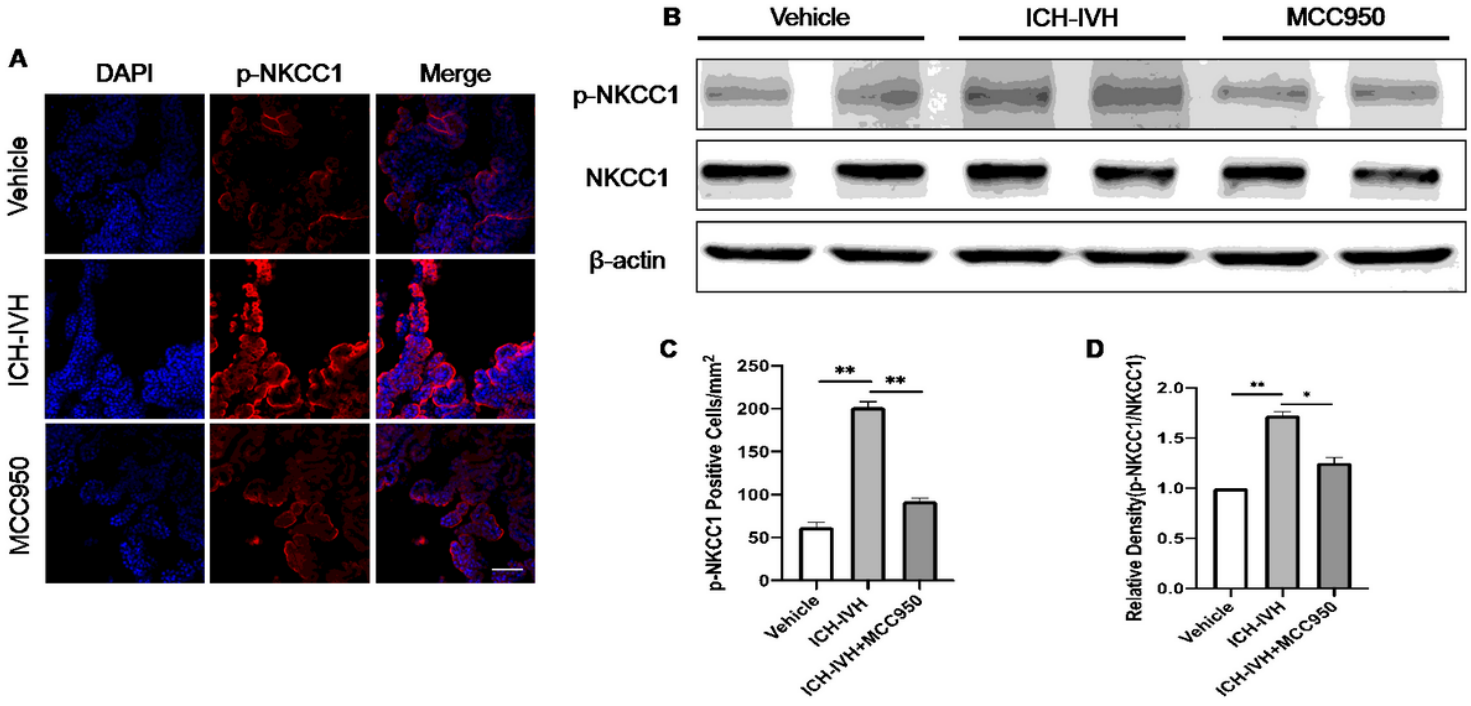

Figure 4

Effects of MCC950 on p-NKCC1 protein expression regulation after ICH-IVH and MCC950 treated. (A, C) Represent photographs of immunofluorescence staining for p-NKCC1 expression (A) and p-NKCC1 positive cells statistics (C) in choroid plexus at 3 days (6 rats/group). Bar=50μm. (B, D) Western blot analysis of p-NKCC1 in choroid plexus at 3 days (6 rats/group). Values are expressed as mean ± SD, **P < 0.01, *P < 0.05.

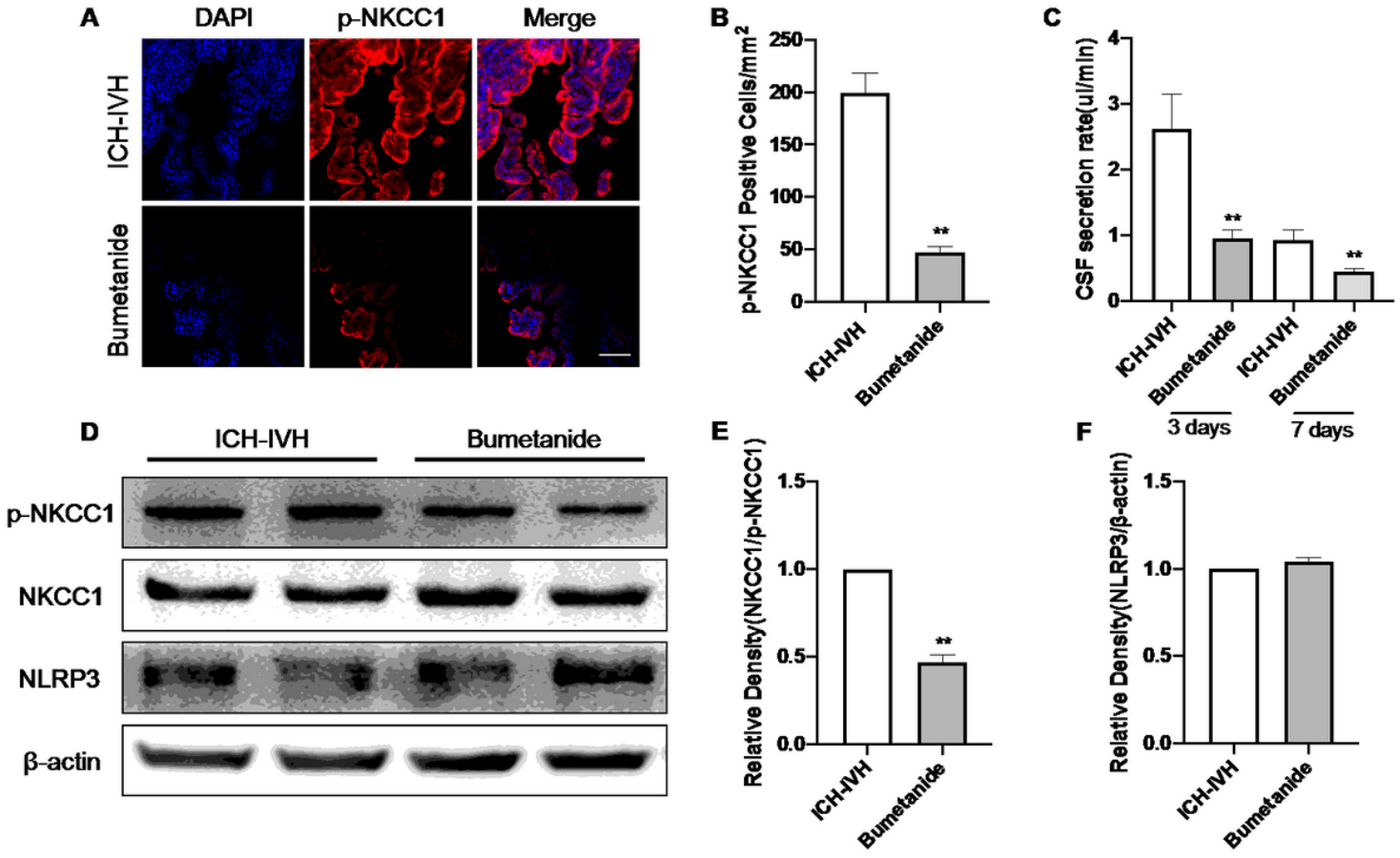

Figure 5

Effects of bumetanide treated after ICH-IVH. (A, B) Represent photographs of immunofluorescence staining for p-NKCC1 expression (A) and p-NKCC1 positive cells statistics (B) in choroid plexus at 3 days following Bumetanide treated (6 rats/group). Bar=50μm. (C) CSF secretion rates after bumetanide treated (6-8 rats/group). (D to F) Western blot analysis of p-NKCC1 and NLRP3 in choroid plexus at 3 days after bumetanide treated (6 rats/group). Values are expressed as mean ± SD, **P < 0.01.

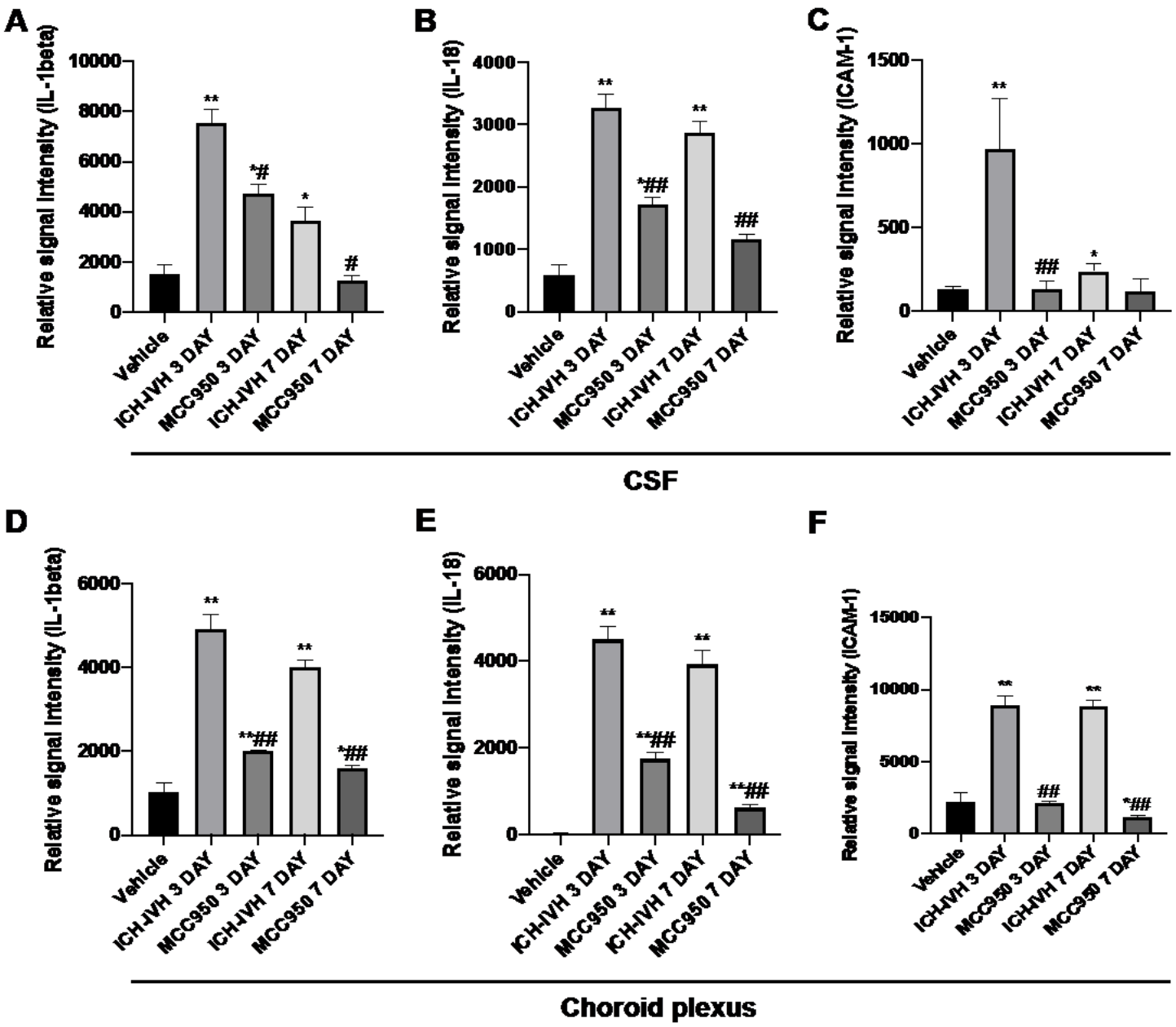

Figure 6

Cytokines changed in choroid plexus and CSF after ICH-IVH. (A to C) Cytokines assay kits analysis of IL-1beta, IL-18, and ICAM-1 expression in CSF. (D to F) Cytokines assay kits analysis of IL-1beta, IL-18, and ICAM-1 expression in choroid plexus. Values are expressed as mean ± SD, **P < 0.01 and *P < 0.05 versus vehicle group; ##P<0.01 and #P<0.05 ICH-IVH group versus MCC950 group.

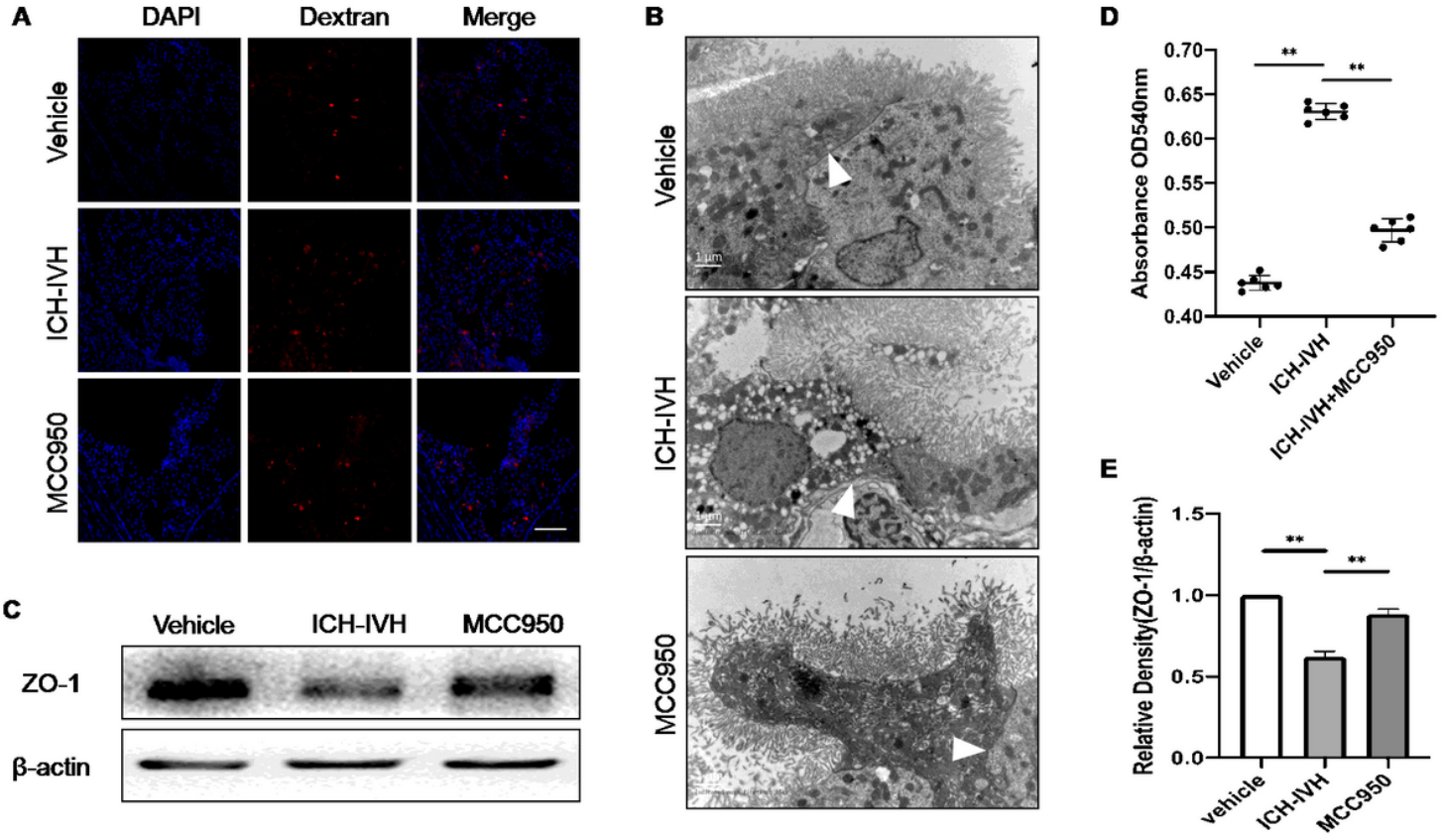

Figure 7

Blood-CSF barrier permeability changed after ICH-IVH in choroid plexus. (A) Represent photographs of Dextran-10,000 MW leakage at 3 days in each group (6 rats/group). Bar=50μm. (B) Represent images of TEM for tight junction between choroid plexus epithelial cells at 3 days in each group (6 rats/group). (C, E) Western blot analysis of ZO-1 expression in choroid plexus at 3 days (6 rats/group). (D) CSF absorbance at 540 nm at 3 days after surgery (6-8 rats/group). Values are expressed as mean ± SD, **P < 0.01. The white arrows show tight junction in choroid plexus.

Supplementary Files

This is a list of supplementary files associated with this preprint. Click to download.

- Fig.S1.tif